Elastic anomalies associated with structural and magnetic phase transitions in single crystal hexagonal $YMnO_3$

2014 J. Phys.: Condens. Matter 26 045901

(http://iopscience.iop.org/0953-8984/26/4/045901)

OPEN ACCESS
IOP Publishing
Journal of Physics: Condensed Matter
J. Phys.: Condens. Matter **26** (2014) 045901 (9pp)
doi:10.1088/0953-8984/26/4/045901

Elastic anomalies associated with structural and magnetic phase transitions in single crystal hexagonal $YMnO_3$

R I Thomson[1], T Chatterji[2], C J Howard[1,3], T T M Palstra[4] and M A Carpenter[1]

[1] Department of Earth Sciences, University of Cambridge, Downing Street, Cambridge, CB2 3EQ, UK
[2] Institut Laue-Langevin, B P 156, F-38042 Grenoble Cedex 9, France
[3] School of Engineering, University of Newcastle, NSW 2308, Australia
[4] Materials Science Centre, University of Groningen, Nijenborgh 4, 9747 At, Groningen, The Netherlands

E-mail: mc43@cam.ac.uk

Received 26 August 2013, in final form 27 October 2013
Published 6 January 2014

Abstract

Resonant ultrasound spectroscopy has been used to measure the elastic and anelastic behaviour through known structural and magnetic phase transitions in single crystal hexagonal $YMnO_3$. Anomalous elastic behaviour is observed at the high temperature structural transition at ~1260 K, with a discontinuity in the elastic constants and nonlinear recovery below T_c, consistent with $\lambda e Q_s^2$ coupling. There is no change in dissipation associated with this high temperature transition, and no evidence in the elastic or anelastic behaviour for any secondary transition at ~920 K, thus supporting the thesis of a single high temperature transformation. Elastic stiffening is observed on cooling through T_N, in accordance with previous studies, and the excess elastic constant appears to scale with the square of the magnetic order parameter. The strains incurred at T_N are a factor of ~20 smaller than those at the structural transition, implying very weak $\lambda e Q_m^2$ coupling and a dominant contribution to the variation in the elastic constants from $\lambda e^2 Q_m^2$. The increased acoustic dissipation above T_N is consistent with an order–disorder process.

(Some figures may appear in colour only in the online journal)

1. Introduction

Some of the most successful examples of magnetoelectric multiferroics have come from the hexagonal rare earth manganites, $RMnO_3$, and significant research has been undertaken to understand the magnetic and ferroelectric properties of these compounds (see, for example, [1–8]). Of these materials $YMnO_3$, with a layered structure with Y ions placed between sheets of corner sharing MnO_5 triangular bipyramids, has been of particular interest [9–16]. It is ferroelectric (FE) below ~900–1300 K and antiferromagnetic (AFM) below ~75 K [15].

In $YMnO_3$ the polarization of the ferroelectric structure is found to be parallel to the crystallographic c axis while the magnetic moments are located in the ab plane, perpendicular to the c axis. Bilinear coupling between the magnetic (AFM) and ferroelectric order parameters is symmetry forbidden but magnetoelectric effects have nevertheless been observed. In particular, Fiebig *et al* [11] observed coupling of antiferromagnetic and ferroelectric order parameters at the ferroelectric domain boundaries. The explanation for the origin of this magnetoelectric effect has been suggested to be the interaction between ferroelectric (FE) and antiferromagnetic (AFM) domain walls. The opposing polarization of neighbouring FE domains induces a strain at the domain wall while the gradual rotation of the magnetic moments across an AFM domain wall causes a local magnetic moment. These two effects can interact via

the piezomagnetic effect, 'clamping' AFM and FE domain walls together such that any reversal of FE order triggers a reversal of AFM order via the induced strain [8, 11, 17]. Alternatively, theory has shown that 'clamping' of the magnetic and ferroelectric order parameters may be caused by the effect of a Dzyaloshinsky–Moriya interaction, which was found to operate within a domain boundary and cause a reversal of the spin direction across an FE wall [18]. Huang *et al* [9] also observed an anomaly in the dielectric constant at T_N, but this can probably be ascribed [17] to biquadratic coupling, which is always symmetry allowed.

The temperatures of the high temperature phase transitions in hexagonal $YMnO_3$ have been the subject of much debate [3, 14, 19–23]. A symmetry analysis [15, 24, 25] shows that there are three possible paths from the high temperature $P6_3/mmc$ phase to the room temperature ferroelectric $P6_3cm$ phase, summarized in figure 1. Fennie *et al* [25] and Kim *et al* [23] supported the path of a single transition (at ∼1270 K), driven by a K_3 order parameter which couples to a secondary zone centre order parameter (associated with Γ_2^-) to induce ferroelectricity. In contrast to this, some studies [14, 24, 26] have suggested one of the paths that involves an intermediate phase between the paraelectric $P6_3/mmc$ phase and the ferroelectric $P6_3cm$ phase. The most recent powder neutron diffraction data agree with the assessment of a single, continuous high temperature phase transition causing a tripling of the unit cell at ∼1258 K from $P6_3/mmc$ to polar $P6_3cm$ [15]. Ferroelectricity is caused by opposite but unequal motion of neighbouring yttrium atoms and accompanying buckling of the MnO_5 octahedra, and therefore the system is actually ferrielectric [27]. This is in contrast to the usual mechanism for ferroelectricity, as in $BaTiO_3$, where displacements of d^0 ions tend to be dominant, but the coexistence of ferroelectricity and magnetism is precluded due to the absence of unpaired electrons [28]. Gibbs *et al* [15] cast doubt on previous reports that there is an intermediate phase between the $P6_3/mcm$ phase and the $P6_3cm$ phase, but did show some limited evidence for a secondary isosymmetric transition at ∼920 K within the $P6_3cm$ phase which, surprisingly, reduces the polarization of the structure. They suggested that this could be due to polar displacements of the Mn–O equatorial planes, which could be related to an electronic transition involving the hybridization of one of the Y–O bonds. A full list of the previously reported high temperature transition temperatures and the methods used to measure them is given in table 1 of Gibbs *et al* [15]. The high temperature structural phase transition in $YMnO_3$ has been considered further in supporting work [16].

$YMnO_3$ orders antiferromagnetically at ∼75 K, although Néel points between 70 and 80 K have been reported [2, 10, 13]. Antiferromagnetism arises from the Mn^{3+} ions, with $S = 2$ spin state, which make up a single magnetic sublattice. The manganese ions sit in a pseudo-two-dimensional triangular arrangement parallel to the (001) plane, with 120° angles between the moments on neighbouring Mn^{3+} ions [29], and a significant degree of magnetic frustration is revealed by large Weiss–Néel point ratios of ∼10 [2]. The low temperature magnetic structure

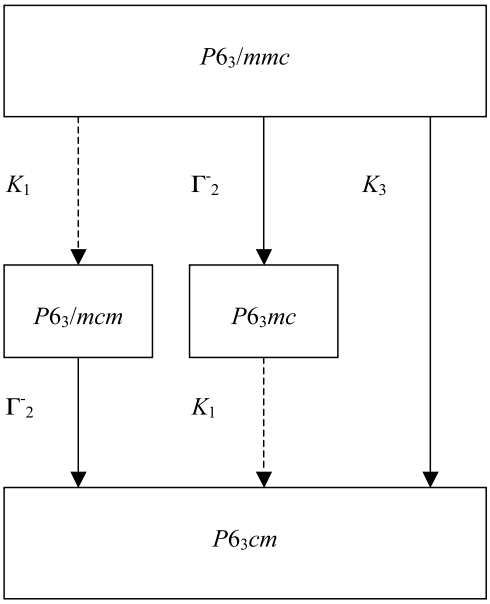

Figure 1. The hierarchy of possible high temperature phase transitions in $YMnO_3$, adapted from Fennie and Rabe [25]. Solid arrows denote transitions that can be continuous and dashed arrows show transitions that must be discontinuous. Arrow labels denote the distortion modes leading to the lower symmetry space group. *K* modes lead to a tripling of the unit cell.

of $YMnO_3$ has never been completely confirmed although current consensus appears to be that it belongs to either $P6_3cm$ or $P6_3'cm'$ which form a homometric pair (magnetic structures that are indistinguishable via neutron diffraction), the latter structure being favoured by optical second harmonic spectroscopy [29–34].

The magnetoelastic coupling effect in $YMnO_3$ has been the subject of much work in recent years and a series of neutron diffraction experiments has been carried out to monitor changes in lattice parameters and atomic positions at T_N [7, 10, 29, 35–37]. Monitoring of changes in atomic positions and bond lengths is difficult due to the small changes involved. This becomes even more complex in a system such as $YMnO_3$ where magnetic structures have the propagation vector $\mathbf{k} = 0$, meaning that magnetic reflections occur at the same position as nuclear reflections, causing great difficulty in the refinement of both magnetic and crystal structures [37]. Lee *et al* [7] observed 'giant' atomic displacements in $YMnO_3$ from neutron and x-ray diffraction experiments and suggested that these displacements could be responsible for coupling of the magnetic and electric order parameters. However, as remarked by Chatterji *et al* [37], no explanation was offered as to how correlations between structural and magnetic parameters were avoided and therefore it is difficult to accept this result. Furthermore, the magnitude of the displacement of the Mn(x) position was 0.01 Å, which is within the spread of reported positions at room temperature (∼0.015 Å), as summarized in table 1.

Poirier *et al* [40] performed low temperature ultrasonic measurements to obtain values for four out of the five elastic constants of hexagonal $YMnO_3$ and found there to be stiffening of all of them on cooling through T_N. The

Table 1. Variation in reported room temperature Mn(x) position.

Reference	Mn(x) position
[38]	0.324 72
[15]	0.317 7(9)
[35]	0.333 0(17)
[29]	0.320 8(18)
[39] (at 10 K)	0.333 5(6)

largest amount of stiffening was observed for C_{66} (∼3%) and C_{11} (∼1%), in comparison with C_{33} and C_{44} (<0.1%), corresponding to a stronger influence of magnetic interactions directed within the (001) plane rather than perpendicular to it. Using a Landau description the relevant strain/order parameter coupling term was determined to be $\lambda e^2 S_\perp^2$, where e is a strain, λ is a strain/order parameter coupling constant, and $S_\perp$ is the in-plane spin component representing the magnetic order parameter. Terms of the form $\lambda e^2 Q_m^2$, where Q_m is a generic magnetic order parameter, are always allowed by symmetry and would lead to stiffening or softening in proportion to Q_m^2, depending on the sign of the coupling coefficient, λ. However, coupling terms $\lambda e_1 Q_m^2$ and $\lambda e_3 Q_m^2$ are also allowed and would be expected to give a stepwise softening at the transition point if the order parameter is able to relax on the timescale of the applied stress. The magnitude of the step scales as $\frac{\lambda^2}{2b}$ for a second order displacive transition, where b is the Landau coefficient for the fourth order term, indicating that if the coupling coefficient λ is small, the amount of softening will also be small. A recent study by Chatterji *et al* [37] allows determination of the magnitude of the strains and has shown that they scale with the square of the magnetic order parameter, refined from neutron diffraction studies, consistent with the expected $\lambda e Q_m^2$ coupling, but also that they are indeed very small.

The aim of this study was to analyse the elastic and anelastic behaviour in $YMnO_3$ below T_N and through the higher temperature transitions using resonant ultrasound spectroscopy (RUS).

2. Experimental methods

The experimental RUS system consists of a single crystal or polycrystalline sample typically cut to the shape of a rectangular parallelepiped being held lightly between two piezoelectric transducers. The first transducer is driven by a frequency synthesizer at constant amplitude across a range of ultrasonic frequencies (0.1–2 MHz) which in turn causes the sample to resonate at particular frequencies. The second transducer acts as a signal detector which records the response of the sample in terms of its displacement when it is vibrated across the frequency range. The data are recorded using Stanford [41] or DRS Modulus II electronics. The vibrational frequencies detected represent the frequencies of the normal modes of the sample. The square of a given peak frequency is directly proportional to the elastic constants associated with that normal mode [42].

The $YMnO_3$ single crystals used in this study were grown by the floating zone technique in air using a four-mirror furnace (Crystal Systems Inc. FZT-10000-H-VI-VP). They belonged to the same batch as described in [43]. The powder used for the single crystal growth was synthesized by sintering stoichiometric amounts of predried Y_2O_3 and MnO_2 at 1200 °C in air. The crystallinity of the boule was verified by Laue diffraction. The crystal used for low temperature RUS experiments was an almost regular parallelepiped with approximate dimensions 5 mm × 4 mm × 3 mm and mass 28 mg. The crystal used for high temperature experiments had an irregular shape with dimensions of the order of ∼4–5 mm and mass 37 mg.

2.1. High temperature

The RUS setup for high temperature measurements consists of two alumina rods mounted horizontally in a Netzsch 1600 °C furnace. The sample is held lightly across a pair of corners between the ends of the rods within the furnace. Piezoelectric transducers are attached to the other ends of the rods outside the furnace. The high temperature apparatus was calibrated against the known alpha–beta transition in quartz [44].

The sample was loaded onto the high temperature head and data were collected during heating and cooling sequences, with an equilibration time of 15 min at each temperature and 20 000 data points collected for each spectrum. Two high temperature sequences were run. The first was from 330 to 830 K in 50 K steps, 830–970 K in 5 K steps, 970–830 K in 5 K steps, 830–330 K in 50 K steps and 330 to 290 K in a 40 K step. The second was from 330 to 1180 K in 50 K steps, 1180–1320 K in 5 K steps and then from 1320 to 1240 K in 5 K steps, 1240–1160 K in 1 K steps, 1160–1140 K in 2 K steps, 1140–330 K in 50 K steps and 330–290 K in a 40 K step.

2.2. Low temperature

In the low temperature head the sample was placed lightly across a pair of faces between the two transducers in a mount which was lowered vertically into a helium flow cryostat, as described by McKnight *et al* [45]. The sample chamber was filled with a few mbar of helium to allow heat exchange between the sample and the cryostat. Two low temperature runs were performed. For the first run the sample was cooled from 280 to 10 K in 30 K steps with a 20 min settle time at each temperature. The sample was then heated from 10 to 30 K in 5 K steps, 30–50 K in 1 K steps and 50–295 K in 5 K steps, with an equilibration time of 15 min at each temperature. For all data collection in this run, 50 000 data points were collected over the frequency range 100–1750 kHz. The second run was performed over the frequency range 100–1600 kHz, again with 50 000 data points per spectrum. The sample was cooled from 275 to 5 K in 30 K steps with a 20 min settle time and then heated from 5 to 65 K in 5 K steps, 65 to 85 K in 2 K steps and 85 to 295 K in 5 K steps, with a 15 min settle time at each temperature.

All spectra were transferred to the software package Igor Pro (WaveMetrics) for analysis. The peak positions and widths at half height were determined for a selection of peaks

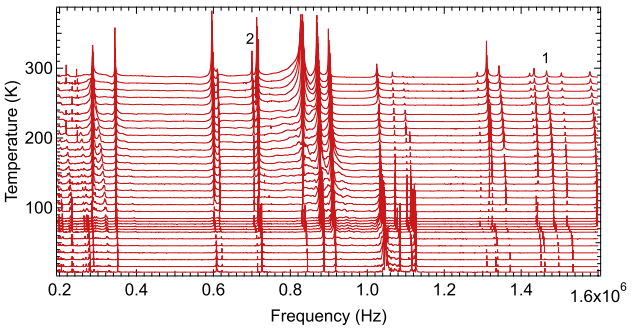

Figure 2. Selected low temperature RUS spectra for $YMnO_3$. The *y*-axis should be amplitude in volts but the spectra have been offset in proportion to the temperature at which they were collected and the axis is therefore labelled as temperature. Peaks **1** and **2** were used to obtain values of f^2 and Q^{-1}.

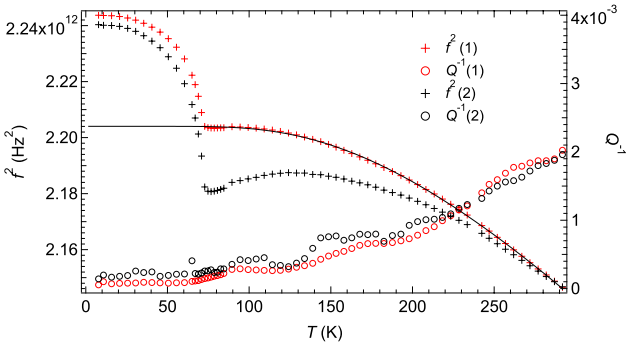

Figure 3. f^2 (crosses) and Q^{-1} (circles) displayed as a function of temperature for peaks **1** (red) and **2** (black) with $f^2(2)$ data scaled to be equivalent to $f^2(1)$ at room temperature. The f^2 data for peak **1** in the temperature range ∼290–75 K have been fitted using equation (1) (shown as a black line) where $a_1 = 2.4 \times 10^{12}$ Hz^2, $a_2 = -7.1 \times 10^8$ Hz^2 and $\theta_s = 317$ K.

by fitting with an asymmetric Lorentzian function. The square of the peak frequency is proportional to the elastic constants associated with that vibrational mode. The quality factor, Q, was calculated using the relationship $Q = f/\Delta f$, where f is the peak frequency and Δf is the width of the peak at half its maximum height. The inverse of the quality factor, Q^{-1}, is a measure of acoustic dissipation in the sample.

3. Results

3.1. Low temperature

Figure 2 shows RUS spectra obtained during heating through the temperature range 8–292 K and stacked in proportion to the temperature at which they were collected. The general behaviour with respect to decreasing temperature is a very slight increase in peak frequency representative of normal elastic stiffening. However, below 75 K, there is an anomalous increase in stiffening, most obvious in less intense peaks at higher frequencies, and saturating as the temperature tends to 0 K.

Many peaks have been analysed over the entire temperature range, recording the square of the peak frequency and the acoustic dissipation. Data from two of these (peaks **1** and **2** in figure 2) are representative and are given in figure 3. On decreasing the temperature from room temperature there is a stiffening of both peaks. In peak **1** stiffening ceases at ∼100 K and there is a very small minimum just above T_N. Below T_N there is a further elastic stiffening which saturates as T approaches 0 K. For peak **2** a very similar evolution is observed except that there is increased softening above the transition temperature, leading to a larger minimum than in peak **1**. An abrupt change in slope occurs for both peaks at 73 K, but the actual minimum of peak **2** occurs at 76.5 K. The patterns of evolution of peaks **1** and **2** are similar to those seen by Poirier *et al* [40] for the elastic constants C_{11} and C_{66} respectively. The acoustic dissipation is extremely low ($Q^{-1} \sim 0.0001$–0.0002) in the lowest temperature range but starts to increase above ∼70 K and continues to rise up to room temperature. There are also possibly some broad features in Q^{-1} at ∼90 and ∼150 K but these are at the level of noise and do not coincide with known anomalies of other properties of $YMnO_3$. Other peaks analysed from figure 2 showed the same stiffening below T_N but showed different amounts of softening on approaching T_N from above.

The excess elastic constant (ΔC) below T_N was determined by fitting a baseline of the form [46]

$$a_0 = a_1 + a_2\theta_s \coth\frac{\theta_s}{T} \quad (1)$$

to f^2 data for peak **1** as shown in figure 3. ΔC values were given by the difference between the data and this baseline, and are displayed in figure 4.

3.2. High temperature

A stack of spectra obtained during cooling is displayed in figure 5. Peaks that vary very little with temperature are caused by resonances of the rods of the high temperature RUS instrumentation. The sample peaks are also weak but they clearly show that on cooling from 1400 K, there is an elastic anomaly at ∼1260 K which involves a softening of the elastic constants. Below this anomaly there is nonlinear stiffening, which is followed by a gentle linear increase in peak frequency down to room temperature consistent with thermal stiffening on cooling.

Figure 6 shows the variation of f^2 and Q^{-1} on heating and cooling for peaks **1** and **2** (as labelled in figure 5), which are representative of the behaviour of other sample peaks. The values of f^2 have been scaled to be in the range 5–7 × 10^{11} Hz^2. Additional data from the second high temperature RUS experiment have been added to this figure to analyse the behaviour through the possible transition at ∼920 K. Since these data are from a different experiment, where it is likely that the sample was held in a slightly different orientation, different resonances were excited and the frequencies have therefore been scaled to overlap with the data from the first experiment. It can be seen that on cooling from high temperatures the anomaly at ∼1260 K is associated with a step in the elastic constants and that there is nonlinear recovery below the transition point. This behaviour represents the

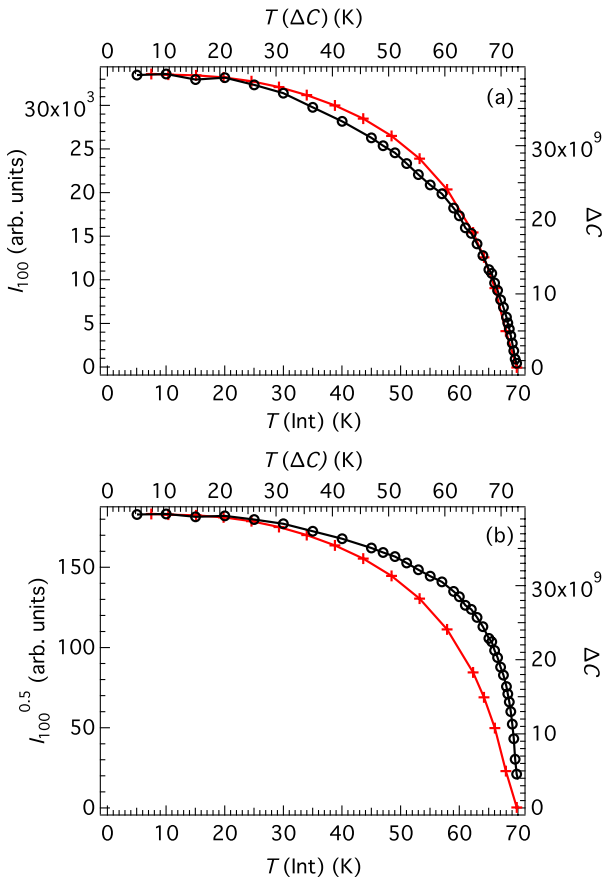

Figure 4. The excess elastic constant from peak **1**, ΔC (red crosses), plotted against temperature. Also shown in (a) are data for the intensity (less the nuclear contribution) of a magnetic ordering reflection ($\propto Q_m^2$) (black circles) from [13] and in (b) the square root of this intensity ($\propto Q_m$) (black circles); these are referred to the left and bottom axes, whereas ΔC is referred to the right and top axes. The temperature axes were adjusted so as to define a common transition point.

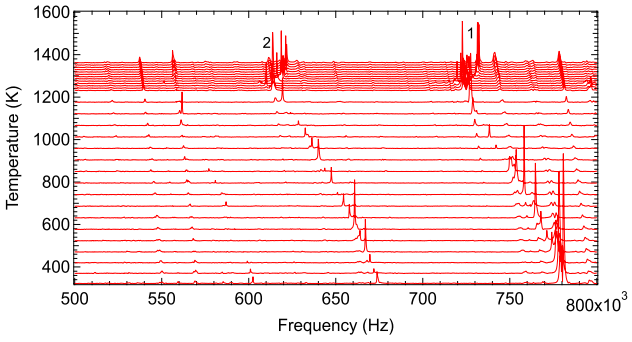

Figure 5. Selected RUS spectra collected during cooling from ~1360 K, offset up the *y*-axis in proportion to the temperature at which they were collected. Peaks analysed for f^2 and Q^{-1} (figure 6) are labelled.

continuous transition from the paraelectric $P6_3/mmc$ space group to polar $P6_3cm$ via a tripling of the unit cell. There is a systematic difference in resonance frequencies on heating and cooling represented by the red and black data respectively, with the sample slightly stiffer on cooling. Figure 6 also shows

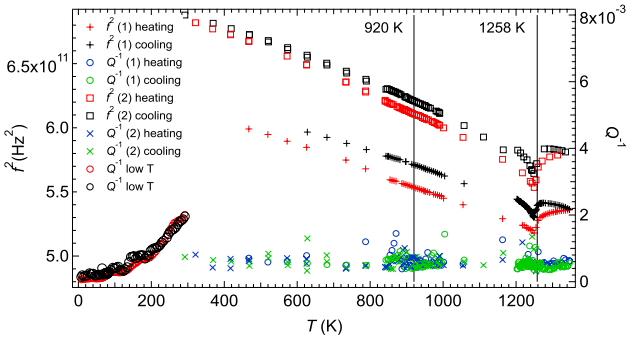

Figure 6. High temperature variation in f^2 and Q^{-1} on heating and cooling for peaks **1** and **2**, as labelled in figure 5. The f^2 data have been scaled to appear in the range 5–7 $\times$ 10^{11} Hz^2. The low temperature variation in Q^{-1} has also been added for comparison. The temperatures of previously reported phase transitions from [15] are added as vertical lines.

the high temperature variation of the acoustic dissipation, and it is apparent that there is essentially no change in Q^{-1} throughout the high temperature range. The low temperature variation in the dissipation has also been added to this plot for comparison, but the step at 300 K is an artefact arising from the different design of the high and low temperature instruments. It is notable that there is no sign of any kind of elastic or anelastic anomaly in the vicinity of 920 K, where Gibbs *et al* [15] suggested an isosymmetric phase transition might be occurring.

4. Strain analysis

In order to understand the elastic anomalies which accompany a phase transition it is usually necessary to first understand the strain behaviour. Lattice parameter data from Lee *et al* [35] and Gibbs *et al* [15] are used here to characterize spontaneous strains arising at both the magnetic ordering transition and the high temperature structural transition. The primary lattice parameter data are reproduced in figure 7(a) with the low temperature data scaled to overlap with the high temperature data. A baseline of the form of equation (1) was fitted to the *a* lattice parameter and the unit cell volume, and a linear baseline was fitted to *c*. The strains $e_1 = e_2, e_3$ and $e_V = 2e_1 + e_3$ were then calculated in the usual manner and are displayed in figure 7(b) [47]. Low temperature strains alone, as obtained by fitting baselines to the primary data between ~80 and ~300 K for *a* and ~80 and ~150 K for *c*, are displayed in figure 7(c).

There is a clear anomaly in all the strains at ~1270–1300 K but no obvious change in behaviour at the reported secondary transition at ~920 K. There is a further deviation at ~80 K which is of much smaller magnitude but of the same sign as the strains derived from higher temperatures. The solid black curve in figure 7(b) represents the solution to a Landau 246 potential (see equation (4) below). This can be written as [48]

$$Q^2 = \frac{1}{2}\frac{-\frac{b}{a} + \sqrt{\left(\frac{b}{a}\right)^2 - 4\frac{c}{a}(T - T_c)}}{\frac{c}{a}}. \qquad (2)$$

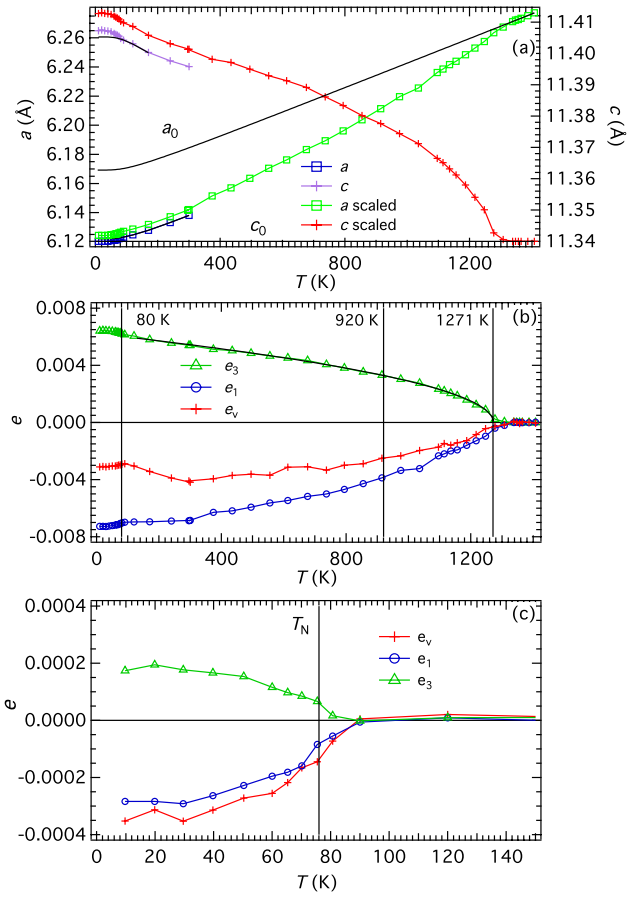

Figure 7. (a) Original low temperature lattice parameter data from Lee *et al* [35] (blue squares and purple crosses) and high temperature data from Gibbs *et al* [15] (green squares and red crosses including scaled low temperature data to allow fitting over the entire temperature range). High temperature fit coefficients (fits made above 1320 K) for a: $a_1 = 6.157$ Å, $a_2 = 8.492 \times 10^{-5}$ Å, θ_s set at 141 K, c: $c_0 = 11.34$–3.014×10^{-5} T and for cell volume (not shown): $a_1 = 370.0$ Å^3, $a_2 = 0.0122$ Å^3, θ_s set at 141 K. (b) Strains e_1, e_3 and e_v as a function of temperature. The curved solid line is a Landau 246 fit to e_3 high temperature data. (c) Low temperature strains alone, calculated from lattice parameter data from [35] (figure 7(a)). Fit coefficients for a: $a_1 = 6.10$ Å, $a_2 = 8.86 \times 10^{-5}$ Å, $\theta_s = 141$ K, c: $a_1 = 11.42$ Å, $a_2 = -7.63 \times 10^{-5}$ Å, θ_s set at 141 K and cell volume: $a_1 = 369$ Å^3, $a_2 = 0.0084$ Å^3, θ_s set at 141 K.

Assuming $e \propto Q^2$ this can be rewritten for the temperature, T, in terms of the strain, e, as

$$T = T_c + Ae^2 + Be. \tag{3}$$

Therefore a polynomial in e_3 was fitted to the data in the interval ∼300–1250 K in figure 7(b) (shown as a solid black curve), which gave a value of $T_c = 1271 \pm 7$ K with coefficients $A \propto \frac{c}{a} = -3.33 \times 10^7$ and $B \propto \frac{b}{a} = 2843$.

Using ISOTROPY [49] a Landau expansion for the sequence of transitions $P6_3/mmc \leftrightarrow P6_3cm \leftrightarrow P6'_3cm'/P6_3cm$ has been produced. It turns out that with respect to the same parent space group, $P6_3/mmc$, the form of the expansion is the same for both transitions, the structural one with K_3 as the active representation and the magnetic one with mK_3. Each would have two order parameter components, q_1 and q_2, giving

$$\begin{aligned} G = {} & \tfrac{1}{2}a(T - T_c)(q_1^2 + q_2^2) \\ & + \tfrac{1}{4}b(q_1^2 + q_2^2)^2 + \tfrac{1}{6}c(q_1^2 + q_2^2)^3 \\ & + \tfrac{1}{6}c'(11q_1^6 + 15q_1^4q_2^2 + 45q_1^2q_2^4 + 9q_2^6) \\ & + \lambda_1(e_1 + e_2)(q_1^2 + q_2^2) + \lambda_3 e_3(q_1^2 + q_2^2) \\ & + \lambda_4(e_4^2 + e_5^2)(q_1^2 + q_2^2) \\ & + \lambda_5[(e_1 - e_2)^2 + e_6^2](q_1^2 + q_2^2) \\ & + \tfrac{1}{4}(C^\circ_{11} + C^\circ_{12})(e_1 + e_2)^2 \\ & + \tfrac{1}{4}(C^\circ_{11} - C^\circ_{12})(e_1 - e_2)^2 + C^\circ_{13}(e_1 + e_2)e_3 \\ & + \tfrac{1}{2}C^\circ_{33}e_3^2 + \tfrac{1}{2}C^\circ_{44}(e_4^2 + e_5^2) + \tfrac{1}{2}C^\circ_{66}e_6^2. \end{aligned} \tag{4}$$

Here a, b and c are normal Landau coefficients, T_c is the critical temperature, the λ are the strain/order parameter coupling coefficients, e_1–e_6 are spontaneous strains and the C°_{ik} are the bare elastic constants (i.e. excluding the influence of the phase transition). The structural transition has $q_1 \neq 0, q_2 = 0$ and the magnetic transition to $P6'_3cm'$ would have $q_1 = 0, q_2 \neq 0$ but $q_1 \neq 0, q_2 = 0$ if the magnetic transition is to $P6_3cm$. In other words, for both transitions there is only one non-zero order parameter component and these can be referred to generically as Q_s and Q_m for the structural and magnetic order parameters respectively. The equilibrium condition $\frac{\partial G}{\partial e} = 0$ gives the strain/order parameter relationships in the usual way as

$$(e_1 + e_2) = \left[\frac{2\lambda_3 C^\circ_{13} - 2\lambda_1 C^\circ_{33}}{(C^\circ_{11} + C^\circ_{12})C^\circ_{33} - 2C^{\circ 2}_{13}}\right] Q^2 \tag{5}$$

$$e_3 = \left[\frac{2\lambda_1 C^\circ_{13} - \lambda_3(C^\circ_{11} + C^\circ_{12})}{(C^\circ_{11} + C^\circ_{12})C^\circ_{33} - 2C^{\circ 2}_{13}}\right] Q^2. \tag{6}$$

The variations of the elastic constants are given in the usual way, following Slonczewski and Thomas [50], Rehwald [51] and Carpenter and Salje [52], and fall into two groups. C_{66} ($= \frac{1}{2}(C_{11} - C_{12})$) and C_{44} have lowest order coupling terms of the form $\lambda e^2 Q^2$ and will therefore vary with the order parameter according to

$$C_{44} = C^\circ_{44} + 2\lambda_4 Q^2 \tag{7}$$

$$C_{66} = C^\circ_{66} + 8\lambda_5 Q^2. \tag{8}$$

$(C_{11} + C_{12})$, C_{13} and C_{33} depend on $\lambda e Q^2$ coupling terms and, for a second order transition, vary as [52]

$$C_{ik} = C^\circ_{ik} - \frac{\lambda^2}{2b}, \tag{9}$$

where λ is the relevant coupling term or combination of coupling terms and b is the fourth order Landau coefficient. The two separate order parameters, Q_s to represent the structural order parameter and Q_m to represent the magnetic order parameter, are necessarily coupled via common strains. In other words, a change in Q_s will induce a change in e_1 which, in turn, must induce a change in Q_m through the $\lambda e_1 Q_s^2$ and $\lambda e_1 Q_m^2$ terms. The same applies to e_3 and the effective

coupling is biquadratic, $\lambda Q_s^2 Q_m^2$, which is also the form of the lowest order direct coupling term allowed by symmetry.

5. Discussion

5.1. High temperature behaviour

$T_c = 1271$ K from the 246 Landau fit to strain data derived from [15] (figure 7(b)) is close to the temperature of the minimum from f^2 data from RUS (~1250 K, figure 6), allowing for the fact that different $YMnO_3$ samples were investigated. The $P6_3/mmc \leftrightarrow P6_3cm$ transition thus displays the standard pattern of elastic softening associated with a phase transition which is co-elastic with respect to strain. Softening ahead of the transition occurs over a limited temperature interval of a few 10s of K and must arise from coupling of acoustic modes with dynamical clusters/fluctuations/short-range ordering. The step arises from coupling terms of the form $\lambda e_1 Q_s^2$ and $\lambda e_3 Q_s^2$, and the nonlinear recovery below T_c is due to the contributions of the sixth order term. The maximum strains are ~0.006, and the maximum softening is ~4%. Without, say, heat capacity data through the transition it is not possible to calibrate the Landau coefficients and produce a quantitative prediction for softening of each of the single crystal elastic constants, but the overall picture is of a classical structural phase transition which conforms to the expected behaviour of a transition which is between second order and tricritical in character. There is no microstructure associated with a co-elastic transition (no symmetry-breaking shear strain) which would move under the application of an external stress. The lack of acoustic dissipation associated with the transition is therefore also entirely consistent with this picture. At least within experimental noise levels there appears to be no evidence for a peak in Q^{-1} at T_c that would indicate coupling of strain to any intrinsic aspect of the transition which might be expected to show critical slowing down as $T \rightarrow T_c$.

Gibbs *et al* [15] suggested the presence of an isosymmetric phase transition at ~920 K, based on changes in equatorial O(z) coordinates and an increase in the equatorial oxygen plane tilt which would lead to a decrease in the polarization. If there are significant atomic displacements associated with this transition it would be expected to couple with strain and be evident in the variation of the elastic constants. From the present study there is no evidence in the elastic behaviour for any transition in the temperature region ~1100–400 K. Additionally, there is no variation in Q^{-1} associated with this temperature interval. If there really is a phase transition in the vicinity of 920 K it is not coupled to any detectable extent with the strain.

The difference in the elastic constants on heating and cooling implies that there is some irreversible change occurring at high temperature which causes the sample to become elastically stiffer. This may be related to impurities in the sample formed by oxidation at elevated temperatures causing small amounts of Y_2O_3 to be formed.

5.2. Low temperature behaviour

The present data from RUS at ~1 MHz for low temperatures are entirely consistent with previous data from pulse-echo ultrasonic measurements at 103 MHz. In both cases there is stiffening associated with the magnetic ordering, apart from the small amount of softening ahead of the Néel temperature. Deformational modes excited in an RUS experiment involve primarily shearing motions, and the variations of f^2, particularly for the lowest frequency modes, are therefore determined by individual, or combinations of, shear elastic constants. Poirier *et al* [40] reported values of C_{66} ($= \frac{1}{2}(C_{11} - C_{12})$) = 59.4 GPa and $C_{44} = 98.6$ GPa at 4 K, and it seems likely, therefore, that the lowest frequency (softest) modes are determined predominantly by C_{66}. The variation of f^2 for peak **2** in figure 3 closely reproduces the variation of C_{66}, with total stiffenings below T_N of ~2.8% (peak **2**) and ~3.1% (C_{66} from Poirier *et al*) respectively. Peak **1** probably also involves C_{66} mixed in with other components, but all the other peaks show f^2 variations which are similar to these. Some of the resonances at least must also involve contributions from C_{11}, C_{12} and C_{33}, so the initial expectation would be that some should involve a degree of softening below T_N. However, the strain analysis shows that the maximum values of the spontaneous strains due to magnetic ordering are only ~0.0003, which is a factor of 20 smaller than the strains coupled with the structural order parameter. Assuming as a first approximation that all other Landau coefficients in equation (4) have approximately the same values for both transitions yields the prediction that the square of the coupling coefficients, and hence the softening, should be a factor of 400 times smaller than is observed at the structural transition, i.e. ~0.01%. In other words, the contributions from $\lambda e Q_m^2$ terms (equation (9)) are negligibly small and the only detectable change arises from $\lambda e^2 Q_m^2$ terms which lead to variations in elastic constants proportional to Q_m^2 (equations (7) and (8)).

The importance of $\lambda e^2 Q_m^2$ coupling was already recognized by Poirier *et al* [40] but can now be tested with improved data for the magnetic order parameter. Intensity data for a magnetic (100) Bragg peak, I_{100}, from Chatterji *et al* [13], corrected for a constant baseline above T_N, have been added to figure 4. Since I_{100} is expected to scale with Q_m^2, the close correlation with the excess elastic constant, ΔC, is consistent with $Q_m^2 \propto \Delta C$. For C_{44} and C_{66}, $\lambda e^2 Q_m^2$ is the lowest order coupling and therefore $Q_m^2 \propto \Delta C$ is expected (equations (7) and (8)). For C_{11} and C_{33} the lowest order coupling is of the form $\lambda e Q_m^2$ but $\lambda e^2 Q_m^2$ is also allowed and will dominate if the former is small, as appears to be the case here.

In figure 8 the reduced I_{100} data are combined with the reduced strains for the magnetic ordering transition alone and confirm $e_i \propto I_{100}$ ($\propto Q_m^2$). The square of the order parameter calculated from the Brillouin function for an $S = 2$ system does not provide a good description of the ordering, however. The character of the transition is complicated by the geometrical frustration and evidence for significant spin fluctuations [3, 40, 53], but both the strain evolution and

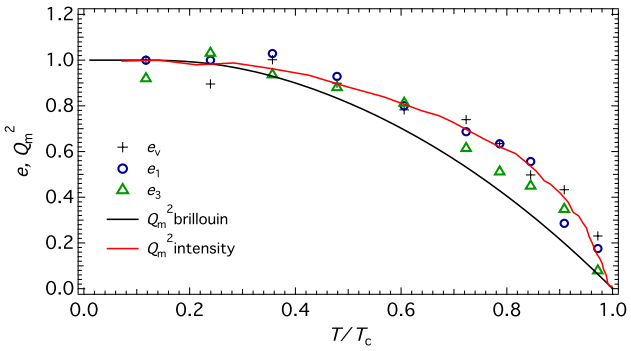

Figure 8. The strains e_1, e_2 and e_v as a function of temperature, calculated from lattice parameter data from Lee *et al* [35] using equation (1), shown against I_{100} from Chatterji *et al* [13], with all data scaled to vary between 0 at T_N and 1 at 0 K, as well as the square of the Brillouin function for an $S = 2$ system.

the elastic stiffening are consistent with a classical coupling model. Furthermore, the extremely weak coupling of Q_m with e_1 and e_3 would contribute only minimally to the biquadratic coupling between the antiferromagnetic and structural order parameters. The lack of acoustic dissipation below T_N points to the absence of any microstructure or fluctuations on a MHz timescale which might couple with strain. Above T_N the very slight increase in Q^{-1} implies that some aspect of the dynamic (magnetic) disordering is coupling very weakly with acoustic mode(s).

It is worth pointing out also that the data presented here show no evidence of piezomagnetic contributions to the measured elastic properties. A bilinear strain/order parameter coupling term is permitted by symmetry for piezomagnetic materials, such as $YMnO_3$, below T_N. The terms to be added to the Landau expansion would be of the form $[M_x(e_1 - e_2) - e_6 M_y]Q_m$, where Q_m is the antiferromagnetic order parameter and M_x and M_y are components of the magnetization induced by strains $(e_1 - e_2)$ and e_6 respectively. Applying a strain $(e_1 - e_2)$ should induce a polarization M_x proportional to this strain, which would then lead to a term that can be written $\lambda(e_1 - e_2)^2 Q_m$. Similarly, if a strain e_6 was applied, a polarization M_y proportional to this strain would be induced, and this would then lead to a term of the form $\lambda e_6^2 Q_m$. These would give a contribution to the elastic constants with linear variations in Q_m. If these coupling coefficients were negative a spontaneous distortion of $(e_1 - e_2)$ or e_6 would lower the energy of the system, which does not occur. The coupling coefficients must be positive, therefore, and these terms could contribute to the observed stiffening. If this effect is present in the RUS results, it is hidden by the much larger stiffening effects from $\lambda e^2 Q_m^2$ terms.

6. Conclusion

Resonant ultrasound spectroscopy and Landau theory have been used to analyse high temperature structural and low temperature antiferromagnetic phase transitions in hexagonal $YMnO_3$. Elastic stiffening below T_N confirms the presence of magnetoelastic coupling and the excess elastic constant appears to vary predominantly with the square of the magnetic order parameter, Q_m^2. The absence of softening is attributed to the fact that the coupling of the strains with the magnetic order parameter is extremely weak. Acoustic dissipation is observed to be low in the magnetically ordered state but increases almost linearly with temperature above T_N. This is attributed to some aspect of dynamic magnetic disorder in the paramagnetic phase coupling (weakly) with the strain. At the high temperature unit cell tripling transition, a minimum in the elastic constants is observed with a discontinuity at T_c and nonlinear recovery of the elastic constants below the transition temperature. This is consistent with coupling to a macroscopic order parameter which evolves at a transition that is intermediate between second order and tricritical in character. No evidence was found for an additional transition at ~920 K, consistent with the view of a single continuous structural transition ($P6_3/mmc \leftrightarrow P6_3cm$) at $T_c \approx 1260$ K.

Acknowledgment

The RUS facilities in Cambridge were established through a grant from the Natural Environment Research Council of Great Britain (Grant no. NE/B505738/1).

References

[1] Tomuta D G, Ramakrishnan S, Nieuwenhuys G J and Mydosh J A 2001 The magnetic susceptibility, specific heat and dielectric constant of hexagonal $YMnO_3$, $LuMnO_3$ and $ScMnO_3$ *J. Phys.: Condens. Matter* **13** 4543–52

[2] Katsufuji T, Mori S, Masaki M, Moritomo Y, Yamamoto N and Takagi H 2001 Dielectric and magnetic anomalies and spin frustration in hexagonal $RMnO_3$ (R = Y, Yb, and Lu) *Phys. Rev.* B **64** 104419

[3] Katsufuji T *et al* 2002 Crystal structure and magnetic properties of hexagonal $RMnO_3$ (R = Y, Lu, and Sc) and the effect of doping *Phys. Rev.* B **66** 134434

[4] Lottermoser T, Lonkai T, Amann U, Hohlwein D, Ihringer J and Fiebig M 2004 Magnetic phase control by an electric field *Nature* **430** 541–4

[5] Lottermoser T and Fiebig M 2004 Magnetoelectric behaviour of domain walls in multiferroic $HoMnO_3$ *Phys. Rev.* B **70** 220407

[6] Zhou J S, Goodenough J B, Gallardo-Amores J M, Moran E, Alario-Franco M A and Caudillo R 2006 Hexagonal versus perovskite phase of manganite $RMnO_3$ (R = Y, Ho, Er, Tm, Yb, Lu) *Phys. Rev.* B **74** 014422

[7] Lee S *et al* 2008 Giant magneto-elastic coupling in multiferroic hexagonal manganites *Nature* **451** 805–8

[8] Wang Z, Huang F Z, Lu X M and Zhu J S 2010 Effect of piezomagnetism on coupling of electric and magnetic domain walls in hexagonal manganites *Eur. Phys. J.* B **75** 217–21

[9] Huang Z J, Cao Y, Sun Y Y, Xue Y Y and Chu C W 1997 Coupling between the ferroelectric and antiferromagnetic orders in $YMnO_3$ *Phys. Rev.* B **56** 2623–6

[10] Park J, Kong U, Pirogov A, Choi S I, Park J-G, Choi Y N, Lee C and Jo W 2002 Neutron-diffraction studies of $YMnO_3$ *Appl. Phys.* A **74** s796–8

[11] Fiebig M, Lottermoser T, Frohlich D, Goltsev A V and Pisarev R V 2002 Observation of coupled magnetic and electric domains *Nature* **419** 818–20

[12] Fiebig M, Goltsev A V, Lottermoser T and Pisarev R V 2004 Structure and interaction of domain walls in $YMnO_3$ *ICM*

2004: Int. Conf. Magnetism (Rome, Jul–AUG.2003) J. Magn. Magn. Mater. **272** (Part 1 Sp. Iss. SI) 353–4
[13] Chatterji T, Ghosh S, Singh A, Regnault L P and Rheinstädter M 2007 Spin dynamics of $YMnO_3$ studied via inelastic neutron scattering and the anisotropic Hubbard model *Phys. Rev.* B **76** 144406
[14] Nénert G, Pollet M, Marinel S, Blake G R, Meetsma A and Palstra T T M 2007 Experimental evidence for an intermediate phase in the multiferroic $YMnO_3$ *J. Phys.: Condens. Matter* **19** 466212
[15] Gibbs A S, Knight K S and Lightfoot P 2011 High-temperature phase transitions of hexagonal $YMnO_3$ *Phys. Rev.* B **83** 094111
[16] Howard C J, Campbell B J, Stokes H T, Carpenter M A and Thomson R I 2013 *Acta Crystallogr.* B **69** 534–40
[17] Goltsev A V, Pisarev R V, Lottermoser Th and Fiebig M 2003 Structure and interaction of antiferromagnetic domain walls in hexagonal $YMnO_3$ *Phys. Rev. Lett.* **90** 177204
[18] Hanamura E, Hagita K and Tanabe Y 2003 Clamping of ferroelectric and antiferromagnetic order parameters of $YMnO_3$ *J. Phys.: Condens. Matter* **15** L103–9
[19] Lukaszew K and Karutkal J 1974 X-ray investigations of crystal-structure and phase transitions of $YMnO_3$ *Ferroelectrics* **7** 81–2
[20] Jeong K, Hur N and Proffen Th 2007 High-temperature structural evolution of hexagonal multiferroic $YMnO_3$ and $YbMnO_3$ *J. Appl. Crystallogr.* **40** 730–4
[21] Kim J, Cho K C, Koo Y M, Hong K P and Shin N 2009 Y–O hybridization in the ferroelectric transition of $YMnO_3$ *Appl. Phys. Lett.* **95** 132901
[22] Choi T, Horibe Y, Yi H T, Choi Y J, Wu W and Cheong S W 2010 Insulating interlocked ferroelectric and structural antiphase domain walls in multiferroic $YMnO_3$ *Nature Mater.* **9** 253–8
[23] Kim J, Koo Y Mo, Sohn K-S and Shin N 2010 Symmetry-mode analysis of the ferroelectric transition in $YMnO_3$ *Appl. Phys. Lett.* **97** 092902
[24] Lonkai T, Tomuta D G, Amann U, Ihringer J, Hendrikx R W A, Tobbens D M and Mydosh J A 2004 Development of the high-temperature phase of hexagonal manganites *Phys. Rev.* B **69** 134108
[25] Fennie C J and Rabe K M 2005 Ferroelectric transition in $YMnO_3$ from first principles *Phys. Rev.* B **72** 100103
[26] Abrahams S C 2009 Atomic displacements at and order of all phase transitions in multiferroic $YMnO_3$ and $BaTiO_3$ *Acta Crystallogr.* B **65** 450–7
[27] Van Aken B B, Palstra T T M, Filippetti A and Spaldin N A 2004 The origin of ferroelectricity in magnetoelectric $YMnO_3$ *Nature Mater.* **3** 164–70
[28] Hill N A 2000 Why are there so few magnetic ferroelectrics? *J. Phys. Chem.* B **104** 6694–709
[29] Munoz A, Alonso J A, Martinez-Lope M J, Casais M T, Martinez J L and Fernandez-Diaz M T 2000 Magnetic structure of hexagonal $RMnO_3$ (R = Y, Sc): thermal evolution from neutron powder diffraction data *Phys. Rev.* B **62** 9498–510
[30] Bertaut E F and Mercier M 1963 Structure magnetique de $MnYO_3$ *Phys. Lett.* **5** 27–9
[31] Bacon G E 1975 *Neutron Diffraction* (Oxford: Clarendon) pp 488–95
[32] Fiebig M, Frohlich D, Kohn K, Leute S, Lottermoser T, Pavlov V V and Pisarev R V 2000 Determination of the magnetic symmetry of hexagonal manganites by second harmonic generation *Phys. Rev. Lett.* **84** 5620–3
[33] Lonkai T, Hohlwein D, Ihringer J and Prandl W 2002 The magnetic structures of $YMnO_{3-\delta}$ and $HoMnO_3$ *Int. Conf. Neutron Scattering (Munich, Sep 2001) Appl. Phys.* A **74** (Part 1, S) S843–5
[34] Lueken H 2008 A magnetoelectric effect in $YMnO_3$ and $HoMnO_3$ *Angew. Chem. Int. Edn* **47** 8562–4
[35] Lee S, Pirogov A, Han J H, Park J-G, Hoshikawa A and Kamiyama T 2005 Direct observation of a coupling between spin, lattice and electric dipole moment in multiferroic $YMnO_3$ *Phys. Rev.* B **71** 180413
[36] Fabreges X, Petit S, Mirebeau I, Pailhes S, Pinsard L, Forget A, Fernandez-Diaz M T and Porcher F 2009 Spin–lattice coupling, frustration, and magnetic order in multiferroic $RMnO_3$ *Phys. Rev. Lett.* **103** 067204
[37] Chatterji T, Ouladdiaf B, Henry P F and Bhattacharya D 2012 Magnetoelastic effects in multiferroic $YMnO_3$ *J. Phys.: Condens. Matter* **24** 336003
[38] Singh A K, Patnaik S, Kaushik S D and Siruguri V 2010 Dominance of magnetoelastic coupling in multiferroic hexagonal $YMnO_3$ *Phys. Rev.* B **81** 184406
[39] Brown P J and Chatterji T 2006 Neutron diffraction and polarimetric study of the magnetic and crystal structures of $HoMnO_3$ and $YMnO_3$ *J. Phys.: Condens. Matter* **18** 10085–96
[40] Poirier M, Laliberté F, Pinsard-Gaudart L and Revcolevschi A 2007 Magnetoelastic coupling in hexagonal multiferroic $YMnO_3$ using ultrasound measurements *Phys. Rev.* B **76** 174426
[41] Migliori A and Maynard J D 2005 Implementation of a modern resonant ultrasounds spectroscopy system for the measurement of the elastic moduli of small solid specimens *Rev. Sci. Instrum.* **76** 121301
[42] Migliori A and Sarrao J L 1997 *Resonant Ultrasound Spectroscopy: Applications to Physics, Material Measurements and Nondestructive Evaluation* (New York: Wiley)
[43] Nugroho A A, Bellido N, Adem U, Nenert G, Simon C, Tjia O M, Mostovoy M and Palstra T T M 2007 *Phys. Rev.* B **5** 174435
[44] McKnight R E A, Moxon T, Buckley A, Taylor P A, Darling T W and Carpenter M A 2008 Grain size dependence of elastic anomalies accompanying the alpha–beta phase transition in polycrystalline quartz *J. Phys.: Condens. Matter* **20** 075229
[45] McKnight R E A, Carpenter Michael A, Darling T W, Buckley A and Taylor P A 2007 Acoustic dissipation associated with phase transitions in lawsonite, $CaAl_2Si_2O_7(OH)_2{\cdot}H_2O$ *Am. Mineral.* **92** 1665–72
[46] Salje E K H, Wruck B and Thomas H 1991 Order-parameter saturation and low temperature extension of Landau theory *Z. Phys.* B **82** 399–404
[47] Salje E K H 1990 *Phase Transitions in Ferroelastic and Co-Elastic Crystals* (Cambridge: Cambridge University Press)
[48] Ballaran T B, Angel R J and Carpenter M A 2000 High-pressure transformation behaviour of the cummingtonite-grunerite solid solution *Eur. J. Mineral.* **12** 1195–213
[49] Stokes H T, Hatch D M and Campbell B J 2007 *Isotropy* (http://stokes.byu.edu/isotropy.html)
[50] Slonczewski J C and Thomas H 1970 Interaction of elastic strain with the structural transition of strontium titanate *Phys. Rev.* B **1** 3599–608
[51] Rehwald W 1973 Study of structural phase-transitions by means of ultrasonic experiments *Adv. Phys.* **22** 721–55
[52] Carpenter M A and Salje E K H 1998 Elastic anomalies in minerals due to structural phase transitions *Eur. J. Mineral.* **10** 693–812
[53] Park J, Park J-G, Jeon G S, Choi H-Y, Lee C, Jo W, Bewley R, McEwen K A and Perring T G 2003 Magnetic ordering and spin-liquid state of $YMnO_3$ *Phys. Rev.* B **68** 104426